Whole-ganglion imaging of voltage in the medicinal leech

using a double-sided microscope

Yusuke Tomina[1] and Daniel A. Wagenaar[1]

[1]Division of Biology and Biological Engineering

California Institute of Technology

Caltech 139-74, Pasadena, California, 91125 USA

Correspondence to: Dr. Yusuke Tomina, Division of Biology and Biological Engineering, California Institute of Technology, Caltech 139-74, Pasadena, California, 91125 USA. E-mail: tominaye@caltech.edu

1   **Abstract**

2   Studies of neuronal network emergence during sensory processing and motor

3   control are greatly promoted by technologies that allow us to simultaneously record the

4   membrane potential dynamics of a large population of neurons in single cell resolution.

5   To achieve whole-brain recording with the ability to detect both small synaptic

6   potentials and action potentials, we developed a voltage-sensitive dye (VSD) imaging

7   technique based on a double-sided microscope that can image two sides of a nervous

8   system simultaneously. We applied this system to the segmental ganglia of the

9   medicinal leech. Double-sided VSD imaging enabled simultaneous recording of

10 membrane potential events from almost all of the identifiable neurons. Using data

11 obtained from double-sided VSD imaging we analyzed neuronal dynamics in both

12 sensory processing and generation of behavior and constructed functional maps for

13 identification of neurons contributing to these processes.

14

15

16

17

1   **Introduction**

2   One of the principal goals in neuroscience is to clarify how neuronal circuits

3   process sensory information and control behavior. Sensory information and behavioral

4   states are represented as dynamic activity patterns of neuronal populations in large

5   neuronal networks. To clarify the neuronal mechanisms underlying sensory processing

6   and behavioral generation, it is necessary to determine which neurons are involved in

7   functionally relevant neuronal dynamics and how those neuronal components interact

8   with each other within the larger network. Technological advances in neuroimaging

9   have enabled brain-wide recording of neuronal activity with sufficiently fine spatial

10   resolution to identify individual neurons within a population[1]. Researchers can perform

11   pan-neuronal Ca^{2+} imaging in selected animals with small size nervous systems,

12   including larval zebrafish [1] and *C*. *elegans* [2-4].

13   Although Ca^{2+} imaging is a convenient tool for detecting neuronal activity, it

14   is limited to intracellular events that are associated with a change in Ca^{2+} concentration.

15   Thus, Ca^{2+} imaging measures neither subthreshold depolarizing nor hyperpolarizing

16   synaptic events. Accordingly, it is difficult to observe synaptic integration processes

17   using Ca^{2+} indicators. In contrast, voltage sensitive dyes (VSDs) can detect both action

18   potentials and sub-threshold excitatory and inhibitory synaptic potentials. VSDs have

19   enabled neuroscientists to examine ethologically relevant neuronal dynamics and to

20   functionally map parts of the nervous systems of sea slugs[5-7] and the medicinal leech

1 *Hirudo verbana* [8-10]. The segmental ganglion of the leech is particularly well suited for

2 comprehensive recording using VSD imaging for two reasons: It consists of only about

3 400 identifiable neurons [11] arranged in a well-preserved geometry in a single spherical

4 shell surrounding a central neuropil, and it functions as a basic unit of sensory

5 processing and control of several behaviors [12]. In the leech segmental ganglion, multiple

6 neuronal circuits responsible for reflexive and voluntary locomotor behaviors have

7 already been characterized by electrophysiology and VSD imaging [8-10, 12]. However,

8 existing technology only allowed imaging one side of a ganglion at a time, and hence

9 captured the activity of at most half of the full ensemble of neurons.

10   To overcome this limitation, we developed a double-sided microscope for

11 VSD imaging, consisting of precisely aligned upright and inverted fluorescent

12 microscopes. This microscope enabled us to record from all cell bodies of a leech

13 ganglion regardless of their location, and allowed us, for the first time, to directly

14 analyze functional relationships between neurons located on opposite surfaces. We

15 combined this double-sided neuronal imaging system with simultaneous

16 electrophysiological recording and stimulation, which allowed us to monitor motor

17 outputs, to verify agreement of VSD signals with actual membrane potentials, and to

18 activate or inhibit selected target cells by injecting current.

19   To demonstrate the utility of the newly developed VSD imaging method, we

20 addressed the following two questions. (1) How are individual identifiable neurons that

21 exhibit higher discriminability for the different sensory stimuli distributed across

4

1   different surfaces of the ganglion? (2) To what extent are neural circuit components

2   unique or shared between different behaviors?

3

4   **Results**

5   *VSD imaging using double-sided microscopy system*

6   Double-sided VSD imaging requires simultaneously focusing two fluorescent

7   microscopes. We achieved this by mounting the fluorescence train of an Olympus BX

8   upright microscope with a custom focus rack on top of the body of an Olympus IX

9   inverted microscope. Both microscopes were equipped with 20x objectives. An

10   optically stabilized high-power LED [13] provided excitation light through the top

11   objective, which operated in epifluorescence mode. The top objective also functioned as

12   a condenser lens for imaging with the bottom objective, which thus operated in

13   transfluorescence mode (Fig. 1a). Because of the high NA of the top objective,

14   inhomogeneities in the imaged tissue did not cause substantive deviations from uniform

15   illumination of the bottom focal plane.

16   The two microscopes were first coarsely aligned (to within about 200 μm) by

17   moving the upright microscope's body and its objective turret, after which

18   micro-alignment was achieved by fine-tuning the position of the upright microscope's

19   objectives in their turret. We used highly sensitive CCD cameras (Photometrics

20   QuantEM 512SC) to image neuronal activity with single cell resolution throughout the

1   ganglion (Fig. 1b). We suppressed mechanical vibration noise by replacing the internal

2   fans of the CCD cameras with external blowers. Photon noise was not substantially

3   different between the top and the bottom image (Top: 72 ± 3 ppm; Bottom: 65 ± 3 ppm

4   (mean $\pm$ SEM over 10 areas size-matched to typical cells).

5   We imaged neural activity with a new-generation voltage sensitive dye,

6   VF2.1(OMe).H [14], which is sensitive enough to record subthreshold events and fast

7   enough to detect action potentials with accurate timing. The dye was loaded into

8   somatic membranes on both aspects of a ganglion by bath application and a perfusion

9   pump for targeted delivery [8]. In leech ganglia, the sensitivity reached $2.7\% \pm 0.3\%$

10   (mean $\pm$ SD across five ganglia in two leeches) at resting potential (-50 mV)

11   (Supplementary Fig.1). Microscopic motion artifacts can have outsized effects on VSD

12   signals compared to Ca^{2+} signals because of the limited relative change in fluorescence

13   of VSDs and their location in the cell membrane. Accordingly, we applied a custom

14   motion correction algorithm to all imaging data (Supplementary Fig.2 & Materials and

15   Methods). Bleaching artifacts in the optical signals were corrected using locally fitted

16   cubic polynomials [15] (Supplementary Fig.3) and global fluctuations were subtracted

17   away [16] (Materials and Methods). The voltage sensor faithfully detected various types of

18   membrane potential change, including action potentials, excitatory and inhibitory

19   postsynaptic potentials, and rhythmic oscillation during fictive behaviors (Fig. 1d).

6

1

2   *Panneuronal VSD imaging and functional mapping based on coherence analysis*

3   We established a mapping between cells seen in the fluorescent images (Fig.

4   1b) and identified neurons on a canonical map (Fig. 1c) using a semi-automated

5   procedure in a custom user interface (Materials and Methods). One of the major

6   advantages of VSDs is that recorded traces can be directly compared to intracellular

7   voltage recordings. This allowed us to identify selected cells in our recordings by

8   comparing our data to previously published intracellular activity of those neurons in the

9   same behaviors.

10   Optically recorded signals simultaneously recorded from both sides of the

11   ganglion closely matched typical patterns of fictive behaviors that have been previously

12   well characterized by electrophysiology and single-sided VSD imaging[9, 12]. We first

13   focused on fictive swimming, which we induced by electrically stimulating a DP nerve

14   root of a posterior ganglion[9] (typically, M13). We then imaged ganglion M10 with our

15   double-sided microscope and simultaneously recorded intracellularly from selected cells

16   (Fig. 2a). Rhythmic activity associated with swimming was readily observed, and we

17   determined which cells were involved in this rhythm by calculating the phase and

18   magnitude of coherence[9] for each cell at the frequency with the greatest spectral power

19   in the rhythm (Fig. 2b, c). The optical signal of dorsal inhibitor motor neuron DI-1

20   exhibits a well-understood swimming oscillation and was used as the phase reference

7

1 for other cells. Using the VF2.1(OMe).H dye, we were able to confirm the oscillatory

2 behavior of neurons previously studied using an earlier-generation dye [9]. In addition, we

3 were able to detect weaker oscillations in many other neurons on both sides of the

4 ganglion.

5 Results from coherence analysis obtained from doubly desheathed ganglia

6 imaged using either camera in our double-sided microscope closely matched results

7 from conventional single-sided imaging, as evidenced by the consistency of the

8 coherence maps computed from either method (Fig. 2b and Supplementary Fig.4). The

9 measured amplitudes of swim oscillations in motor neuron DI-1, the noise levels in

10 those recordings, and the coherence between bilateral homologues of DI-1 were also

11 indistinguishable between single-sided and double-sided imaging experiments

12 (Supplementary Fig.4), indicating that double-sided imaging does not entail any

13 compromises from an imaging quality perspective.

14

15 *Encoding of stimulus identity by individual neurons*

16 We used double-sided VSD imaging to record the activity of all neurons in

17 isolated single ganglia during a fictive reflexive behavior known as local bending, a

18 withdrawal response to tactile stimulation in which the leech bends its body away from

19 the stimulated location [12]. Local bending can be induced readily in isolated single

20 ganglia by stimulating one of four pressure-sensitive sensory neurons (P cells).

8

1   Stimulating P cells causes a combination of excitation and inhibition in identified "local

2   bend interneurons" (LBIs) [12, 17]. The LBIs synapse onto several motor neurons to

3   produce an appropriate pattern of contraction and relaxation in the local area of the body

4   wall that depends on which location (or which P cell) was stimulated[12, 17, 18].

5   We induced local bending by stimulating the left and right ventral P cells (P_V^L

6   and P_V^R) with trains of depolarizing pulses (20 Hz, 50% duty cycle, 1 s), which reliably

7   evoked action potentials in those cells (Fig. 3a, b). Stimuli were presented in order of

8   LRRLLR…, for a total of 10 stimuli per P cell. From each of the resulting VSD traces,

9   we extracted the average fluorescence change ($\Delta F/F$) during the first 0.5 s of the

10   stimulus as well as during a control phase (1–0.5 s before stimulus onset), both relative

11   to a reference phase (0.5–0.1 s before stimulus onset; Fig. 3c). Using a leave-one-out

12   procedure, we calculated for each of the cells how reliably their activity could be used

13   to "predict" which of the P cells had been stimulated (Fig. 3d). We then established a

14   mapping between cells in the VSD images and identified neurons on the canonical maps

15   to determine for all identified neurons to what degree their activity encoded stimulus

16   identity (Fig. 3e).

17   On average across eight experiments, 113 ± 11 (mean ± SD) cells on the

18   ventral surface and 129 ± 6 on the dorsal surface could be mapped to identified neurons

19   (Fig. 3f). Among those, 28% of ventral cells [35 ± 11, mean ± SD] and 36% of dorsal

20   cells (52 ± 18) encoded stimulus identity with prediction success higher than 75%

21   during the first 0.5 s of the stimulus. This included one ventral LBI, all dorsal LBIs, and

9

1   most motor neurons (MNs; Fig. 3g). (All other ventral LBIs had prediction success in

2   the range 65%–75%. In contrast, the average prediction success in the control period

3   was at chance level: 50.9 % ± 1.3% (mean ± SEM) for both ventral and dorsal cells.)

4   The other neurons with high prediction success were AP cells and Leydig cells, as well

5   as cells provisionally identified as cells 56, 61, 251, and 152 on the ventral surface and

6   cells 9, 10, 22, 28, 107, and 123 on the dorsal surface.

7

8   *Involvement of individual neurons in multiple behaviors*

9   To further establish the utility of double-sided VSD imaging, we set out to

10   determine to what extent neural circuit components are unique or shared between three

11   behaviors: local bending, swimming, and crawling. To do so, we evoked the

12   corresponding fictive behaviors in isolated whole nerve cords using electrical

13   stimulation[9]. Specifically, local bending was activated by intracellular stimulation of a

14   single P_V^L or P_V^R [19]; swimming was elicited by stimulating a DP nerve from either

15   ganglion 11, 12, or 13; and crawling was elicited by stimulating tail brain nerve roots.

16   Motor patterns of local bending and swimming were confirmed based on extracellular

17   recordings of DP nerves or intracellular recording of AE cells[9, 10, 20]. Crawling patterns

18   were confirmed based on by simultaneous intracellular recordings from two different

19   motor neurons: the AE and CV cells[9]. All three behaviors could be induced in each of

20   six animals (Supplementary Videos 1–4).

10

1   We calculated the phase and magnitude of the coherence of each imaged

2   neuron to the stimulus train (0.5 Hz) during local bending; to the optical signal of motor

3   neuron DI-1during swimming; and to the intracellular trace of an AE cell during

4   crawling. Results from all behaviors in one animal are shown in Fig. 4a–d and

5   Supplementary Videos 1–4. Optical signals from representative cells located on both

6   surfaces confirmed stereotyped activity patterns that were highly distinctive for each of

7   the behaviors (Fig. 4e–h).

8   We established identities of imaged neurons as before. On average over six

9   preparations, we were able to assign 126 ±11 cells on the ventral surface and 121±10 on

10   the dorsal surface. This allowed us to construct summary maps showing which neurons

11   were consistently involved in which behaviors (Fig.4j and Materials and Methods).

12   Approximately 10% cells were involved in all three behaviors, 33% in two out of the

13   three behaviors, and 42% in a single behavior (Fig. 4j). For the remaining 15% of cells,

14   involvement in any of the behaviors could not be established.

15   Finally, we calculated a correlation matrix between the recorded activity of

16   each of the cells, separately during each of the three behaviors, and performed

17   automated clustering based on these correlations (Fig. 5a). For each of the cells in a

18   recording, we then calculated what fraction of the cells in the same cluster were located

19   on the ventral or the dorsal side of the ganglion. We found that during crawling and

20   especially during local bending, most clusters were largely confined to only one side of

21   the ganglion, whereas during swimming they more commonly spanned sides (Fig. 5b),

11

1   which indicates that swimming involves correlated activity among cells located on both

2   surfaces whereas local bending largely does not. We quantified this by calculating an

3   "integration coefficient" (Materials and Methods) which is equal to zero if all clusters

4   are either wholly on the dorsal or wholly on the ventral side, and equal to one if all

5   clusters are equally spread between the two sides (Fig. 5c).

6

7   **Discussion**

8   We constructed a double-sided microscope that can record fluorescence

9   signals from two sides of a biological preparation. This technique should be broadly

10   applicable to experimental questions that require simultaneous imaging from two

11   widely spaced cell layers in Drosophila[21], sea slugs[5,6] and other organisms. The optical

12   system can be assembled from conventional optic parts and devices. In our

13   implementation, we used microscope parts from Olympus, but an equivalent system

14   could now be constructed using, e.g., Thorlabs CERNA parts.

15   By combining our microscope with next-generation voltage-sensitive dyes

16   (VF2.1(OMe).H[14], we achieved simultaneous large-scale neuronal recording from two

17   widely spaced cell layers at single-cell resolution, capturing not only action potentials

18   but also small excitatory and inhibitory synaptic potentials. A primary feature of the

19   system is its ability to acquire these signals at high speed, and without delay for image

20   capture between the two focal planes. At present, this cannot be achieved by wide-brain

12

1 volumetric Ca^{2+} imaging as previously established for *C. elegans*[2,3] . With our newly

2 developed microscope, we simultaneously recorded, for the first time, the activity of the

3 majority of neurons in a leech ganglion. While beyond the scope of this study, the fact

4 that VSD recordings contain both spikes and postsynaptic potentials makes it possible

5 to infer network connectivity among the different individual, identifiable cells. This

6 offers a notable advantage over techniques that only give access to spike events or

7 intracellular Ca^{2+} concentration.

8   The leech has 21 nearly identical segmental ganglia containing approximately

9 400 neurons that are arranged in a highly conserved geometry[12]. For 148 of these

10 neurons, functional descriptions have been published. (A gateway to the relevant

11 literature is available online, at http://www.danielwagenaar.net/ganglion.) The

12 ganglionic neurons are distributed in a single layer on the surface of the ganglion, but

13 this layer wraps around both the dorsal and ventral sides, so that at best half of the

14 neurons can be simultaneously imaged with conventional microscopy. Our double-sided

15 microscope, in contrast, has access to all of them, although surface curvature means that

16 not all neurons can simultaneously be in sharp focus (Fig. 1b). A single light source was

17 sufficient for illuminating both top and bottom surfaces, because the leech nervous

18 system is sufficiently translucent to permit even lighting onto both sides.

19   In many leech ganglionic neurons, the somata exhibit both action potentials

20 and synaptic potentials not greatly attenuated from their origin in the neuropil, a notable

21 difference from typical monopolar neurons in invertebrate central nervous systems[12].

13

1   Hence, a low-noise imaging system using sensitive voltage sensors potentially enables

2   us to analyze synaptic integration even in small neurons in the leech. In addition, our

3   double-sided microscope is compatible with both intra- and extracellular electrode

4   placement, enabling detailed electrophysiological interrogation of selected specific

5   neurons along with optical imaging from the population.

6   Intriguing features that we observed using our pan-neuronal imaging system

7   are (1) widespread distribution of neurons that are differentially involved in left and

8   right ventral local bending (Fig. 3c, d), and (2) involvement in multiple behaviors of a

9   large fraction of identifiable neurons (Fig. 4i, j).

10   With respect to (1), we found that not only the local bend interneurons and the

11   motor neurons previously reported[17] discriminate between the stimuli, but so did many

12   other neurons that had not previously been implicated in local bending. It has long been

13   known that the neural mechanism of local bending involves population coding[22-27], but

14   its exact algorithm and computation remain unknown. Although the calculation of

15   discriminability here was based on stimulus category (P_V^L vs. P_V^R) instead of actual

16   local bend patterns in the leech's body wall, the population dynamics of the highly

17   discriminative cells we identified putatively underlie the neuronal computation. The

18   discriminability maps from our study can thus be utilized for future investigations of

19   mechanosensory information processing.

14

1   With respect to (2), we observed that 43% of identifiable neurons on the

2   ventral and dorsal surfaces were involved in at least two of the three behaviors tested

3   (local bending, swimming, and crawling). This result indicates that the neural circuits

4   for those behaviors share many components while generating unique motor patterns for

5   each behavior. The percentage of circuit components shared between swimming and

6   crawling identified in this study differed from previous work[9]; in particular, the number

7   of cells we identified as involved in crawling (56) was lower than in the previous study

8   (188). The reason is probably that crawl episodes in our experiments were somewhat

9   shorter (typically only 3–4 cycles) than in the older study, resulting in a weaker

10   coherence signal. Double-sided imaging revealed a previously unappreciated difference

11   between the swim rhythm and local bending: The cell assemblies that are

12   simultaneously active in the former span both sides of the ganglion, whereas in local

13   bending, they are mostly confined to either the dorsal or the ventral side.

14   In this study, we identified imaged cells with known neurons using a

15   semi-automatic mapping algorithm based on cell size and location along with an

16   expert's assessment based on the physiological properties of cells along with this

17   geometrical information. To gain more insight into the neuronal networks responsible

18   for behavior, it will be necessary to carry out more accurate neurocartography, which

19   we will achieve by combining functional mapping using machine learning methods[10]

20   with a connectomic approach using serial block face scanning electron microscopy[11].

21   The combination of those techniques with double-sided VSD imaging will pave the way

1   for future investigations on how the activity of all neurons in a central nervous system is

2   recruited to process sensory information and to generate distinctive behaviors from

3   overlapping neuronal circuits.

1   **Materials and Methods**

2   *Optical recording by double-sided microscope*

3   We acquired fluorescence images simultaneously from two focal planes using

4   a custom double-sided microscope consisting of the fluorescence train of an upright

5   microscope (Olympus BX, Tokyo, Japan) mounted on top of an inversed microscope

6   (Olympus IX). The top microscope was used to image the upper focal plane while the

7   bottom microscope imaged the lower focal plane. We used a 20x, 1.0 numerical

8   aperture (NA), water-immersion objective for the upright and a 20x, 0.7 NA objective

9   with cover-slip adjustment collar for the inverted microscope (both Olympus). The

10   alignment of those two objectives was fine-adjusted manually so that cameras attached

11   to the top and bottom microscopes saw the same field of view to within about 300 nm

12   when the two focal planes were at the same depth.

13   The two objectives served as condenser for each other, so that blue excitation

14   light delivered through the top objective for epifluorescence imaging also served as a

15   transfluorescence light source for the bottom objective. Further, a red LED illuminator

16   attached to the bottom microscope provided wide-field transillumination that enabled us

17   to use the upright objective to visualize intracellular electrodes. Both objectives were

18   mounted on standard turrets so that they could be rotated out of the way to make place

19   for 5x objectives used to visualize extracellular suction electrodes.

17

1   For VSD imaging, we used excitation light (bandpass filtered to 470 ± 15 nm)

2   from a high-power blue LED (LedEngin LZ1-10B200) controlled with optical

3   stabilization[13]. In both the upright and inverted microscopes, we used a 490-nm dichroic

4   mirror and 505-nm LP emission filter. Images were acquired with two cooled CCD

5   cameras (QuantEM 512SC; Photometrics, Tucson, AZ) at a resolution of 512 x 128

6   pixels. The frame rate was set depending on which behavior was recorded: for local

7   bending and swimming, images were acquired at 50 Hz; for crawling, images were

8   acquired at 20 Hz. Imaging data were acquired using custom software VScope[28]. Optical

9   and electrical recordings were synchronized by connecting frame timing signals from

10   each camera to a data acquisition board that also recorded electrophysiology signals (see

11   below).

12   (ア) VSD imaging is highly sensitive to even sub-micrometer motions. Because

13   VSDs are located in cell membranes rather than the cytosol, a movement of

14   less than 1% of a cell diameter can cause a signal change of well over 1% due

15   to bright edge pixels moving out of a pre-defined region of interest (ROI).

16   Since typical VSD signals are themselves far less than 1%, this can cause

17   dramatic motion artifacts. To mitigate this problem, we replaced cooling fans

18   inside each CCD camera with external blowers, since we determined that

19   internal fans in cameras caused significant vibrations of the microscope

20   objectives relative to the sample. After removing these fans, the noise in

21   image sequences was dominated by shot noise.

1   *Animal maintenance and sample preparation*

2   Medicinal leeches (*Hirudo verbana*) were obtained from Niagara Leeches

3   (Niagara Falls, NY) and maintained in artificial pond water at 15 °C. In experiments

4   where only local bending was the target behavior, we dissected out short chains of

5   ganglia from segments 8 through 12. In experiments involving swimming or crawling,

6   we isolated whole nerve cords (Supplementary Fig 5), including the head brain, all 21

7   segmental ganglia, and the tail brain. In all cases, the blood sinus surrounding the

8   nervous system was dissected away around segmental ganglion 10. We removed the

9   sheath from the ventral and dorsal surface of this ganglion before applying

10 voltage-sensitive dyes. To induce swimming, a dorsal posterior (DP) nerve root in one

11 of ganglia 11 through 13 was stimulated through a suction electrode. Brief electrical

12 pulses (3 ms) were delivered at 50 Hz in a 3-s-long train, with an amplitude of 7–8 V.

13 To elicit crawling, several nerves from the tail brain were stimulated using the same

14 stimulus parameters as for DP nerve stimulation. Isolated leech ganglia can move

15 slightly move because muscle cells are embedding in the nerve cord. We therefore

16 stablized the ganglion to be imaged by tightly pinning down blood sinus tissue to the

17 PDMS (Sylgard 184, Dow Corning, Midland, MI) substrate and by sandwiching

18 adjacent connectives between small pieces of medical dressing (Tegaderm, 3M,

19 Maplewood, MN) which was also pinned down, to minimize any motion artifacts.

20 Throughout the dissection and during imaging, preparations were maintained in

21 chambers filled with cold leech saline consisting of the following (in mM): 115 NaCl, 4

19

1   KCl, 1.8 CaCl2, 2 MgCl2, 10 glucose, and 10 HEPES, at pH 7.4. Only before crawling

2   was induced, we temporarily replaced the cold saline with room temperature (20–23 °C)

3   saline to obtain the most natural crawling rhythm. We bath loaded 800 μM

4   VF2.1(OMe).H [14](provided by Evan Miller) in leech saline containing 1% Pluronic acid

5   (PowerloadTM Concentrate 100x, Thermo Fisher Scientific, Waltham, MA). To help

6   with dye penetration into the cell membranes, we circulated the solution using a pair of

7   peristaltic pumps (approximately 1.1 mL/min flow rate) with outflows directed at the

8   dorsal and ventral surfaces of the ganglion, for 20 minutes total.

9

10   *Electrophysiology*

11   We recorded intracellularly from up to three neurons simultaneously using

12   20–50 MΩ glass microelectrodes filled with 3 M potassium acetate and 60 mM

13   potassium chloride, using Neuroprobe amplifiers (Model 1600; A-M systems, Sequim,

14   WA). Intracellular recordings provided additional information regarding the behavioral

15   state of the preparation as well as confirmation of the corresponding optical signals. We

16   recorded extracellularly using suction electrodes and a four-channel differential

17   amplifier (Model 1700; A-M Systems). All electrical signals were digitized at 10 kHz

18   using a 16-bit analog-to-digital board (NI USB-6221; National Instruments, Austin, TX)

19   and VScope software[28].

1

2   *Basic data processing*

3   We outlined the images of individual cell bodies manually as regions of

4   interest using VScope. Pixel values within each cellular outline were then averaged in

5   each frame, yielding a raw fluorescence signal. Signals were processed to remove

6   artifacts from micromotion (next section), and to correct for slow reduction of overall

7   fluorescence intensity due to dye bleaching. The latter was achieved by subtracting

8   locally fitted third-order polynomials using the SALPA algorithm[15] with a time constant

9   of 1 to 15 s. In addition, brightness averaged across the areas of the ganglion outside of

10   ROIs was subtracted for each frame to reduce global noise due to fluorescent crosstalk

11   among top and bottom images[16]. Finally, signals were normalized to their average value

12   and expressed as a percent change in fluorescence ($\Delta F/F$).

13

14   *Motion correction*

15   As mentioned above, motion artifacts were reduced by removing fans from

16   CCD cameras and by pinning down ganglia tightly on the PDMS substrate. However,

17   even very small motions can cause highly detrimental artifacts in VSD recordings.

18   To correct for small motions, we designated the middle frame of any recording as a

19   reference frame, and generated a pair of artificial frames by shifting the reference frame

21

1   one pixel to the left or to the right. Let $\mathbf{I}_R$ and $\mathbf{I}_L$ be vectors consisting of the intensity

2   values of the pixels in the right- and left-shifted reference frames, and let $\mathbf{I}'$ be the

3   intensity vector of an arbitrary frame in the recording. As long as the motion is small

4   (less than or approximately equal to one pixel),

5    $$\Delta x = 2\,(\mathbf{I}' - \mathbf{I}_L) \cdot (\mathbf{I}_R - \mathbf{I}_L)\,/\,\|\mathbf{I}_R - \mathbf{I}_L\|^2 - 1,$$

6   where · is the vector product and $\|\mathbf{I}\|$ is the vector norm, is a good estimate for the

7   motion in the x-direction between the frame under study and the reference frame. (The

8   reason is that an image shifted by Δx pixels can be approximated as

9    $$\mathbf{I}' = [(1 - \Delta x)\,\mathbf{I}_L + (1 + \Delta x)\,\mathbf{I}_R]\,/\,2,$$

10   as long as $|\Delta x| \lessapprox 1$. The first equation is derived from the second by minimizing with

11   respect to Δx.)

12   The same method can of course be used for motion in the y-direction. More

13   interestingly, the method can be used for other affine distortions as well. For instance, if

14   we calculate artificial frames by rotating the reference frame by $\pm 0.1°$, the above

15   procedure would yield estimates of image rotation (in units of $0.1°$).

16   Using this method, we estimated and corrected for small motions that may

17   occur with the preparation or even due to vibrations in the microscope, thus preventing

18   motion artifacts in the extracted VSD traces (Supplemental Figure 2).

1

2   *Calculation of prediction success*

3   In our experiments on the encoding of stimulus identity by individual neurons,

4   we performed 10 trials stimulating the left P_V cell and 10 stimulating the right P_V cell, in

5   order (LR)(RL)(LR)(RL)… To calculate how well each cell "predicted" the stimulus

6   identity (i.e., "left" or "right"), we calculated the average ΔF/F during the first 0.5 s of

7   each stimulus relative to the preceding reference phase, separately for each trial. Taking

8   each trial in turn, we then took that trial and its "partner" trial out, and calculated the

9   average ΔF/F for the 9 "left" stimuli out of the remaining 18 trials and also for the

10   "right" stimuli. The "partner" trial was the next trial for odd-numbered trials, and the

11   preceding trial for even-numbered trials. If the ΔF/F in the trial under consideration was

12   closer to the average ΔF/F of the "left" trials in the training set than to the average of

13   the "right" trials, the neuron was considered correct in its "prediction" of stimulus

14   identity if the trial under consideration was in fact a "left" trial, and conversely for

15   "right" trials. The percentage of trials in which a cell correctly predicted stimulus

16   identity in this sense was used as a measure of prediction success. Any cell that

17   correctly predicted stimulus identity in at least 75% of trials (50% being change

18   performance) was considered to encode stimulus identity.

1

2   *Coherence analysis*

3   We used multitaper spectral analysis[29] to estimate the coherence between

4   optical signals from individual cells with a common reference. That reference was the

5   stimulus train for local bending, the optical signal of a DI-1 motor neuron for swimming,

6   or the intracellular electrode signal of an AE motor neuron for crawling. For each

7   recording, we calculated the 95% confidence interval for the magnitude of estimated

8   coherence under the null hypothesis that a signal was not coherent with the reference[30].

9   A cell was considered to be involved in the behavior expressed during a given trial if its

10   measured coherence exceeded this confidence interval.

11

12   *Canonical mapping*

13   The overall layout of neurons within leech ganglia is highly conserved

14   between ganglia within an animal as well as between animals, but the precise geometry

15   does vary. In order to identify cells seen in the VSD image sequence (Supplementary

16   Fig.5a) with neurons in the canonical map, we developed a graphical user interface that

17   allows us to proceed as follows. First, we mark all the visible cells as regions of interest

18   on the image (Supplementary Fig.5b). Then, we overlay the canonical map over this

19   (Supplementary Fig.5c). To the trained eye, the identification of many of the larger cells

24

1   is immediately obvious, so we register these identities (using a drag-and-drop

2   mechanism in the GUI; (Supplementary Fig.5d)). This partial mapping of ROIs to

3   identified neurons allows the program to do a coarse alignment between the canonical

4   map and the actual image using affine transformations local to each of the four packets

5   of cells (Supplementary Fig.5e). (The ganglion is divided by giant glial cells into

6   several packets[12], the boundaries of which are indicated on the canonical map.) This

7   preliminary alignment enables us to identify several other neurons with high confidence,

8   after which the computer can perform a local alignment step. Finally, the computer

9   assigns putative identities to the remaining ROIs, leading to a nearly complete mapping

10   between ROIs (orange dots in Supplementary Fig.5f) and identified neurons (cross

11   marks).

12

13   *Determination of which cells are consistently involved in a behavior*

14   For each neuron in each animal, we determined whether its coherence

15   exceeded the 95% confidence interval of the null hypothesis that a given neuron was not

16   involved in a given behavior. If a neuron exceeded that threshold for a given behavior in

17   four out of six animals, it was considered to be involved in that behavior (Fig. 4i.) Since

18   swimming and crawling are both symmetric behaviors, we included both members of a

19   homologous pair if (and only if) at least one member exceeded the 97.5% C.I.

20

1   *Clustering and calculation of integration coefficients*

2   We clustered cells based on the matrix of the correlation coefficients of their

3   activity patterns, separately for each behavior (by constructing a dendrogram based on

4   the correlation distance followed by tree cutting). We then assigned a dorsoventrality

5   index (DVI) to each cell, which was equal to the fraction of dorsally localted cells in

6   that cell's cluster. This is what is shown in the histograms of Fig. 5b. Cells in clusters

7   with fewer than three members were ignored for this calculation; the results did not

8   change qualitatively if this threshold was changed to two or five. Based on the DVI, we

9   calculated the integration coefficient (CI) of Fig. 5c as:

10      $\mathrm{CI} = \langle\, 1 - 2\, |\mathrm{DVI} - \tfrac{1}{2}|\, \rangle$,

11   where $|\cdot|$ denotes absolute value and $\langle\,\cdot\,\rangle$ denotes the average across all cells (except

12   those not in clusters of size three or more).

13

14   *Software for data analysis*

15   All data processing and statistical analysis were performed in GNU Octave,

16   version 4.0.0.

17

18

References

1. Ahrens, M.B., Orger, M.B., Robson, D.N., Li, J.M. & Keller, P.J. Whole-brain functional imaging at cellular resolution using light-sheet microscopy. *Nat. Methods* 10, 413–420 (2013).

2. Schrödel, T., Prevedel, R., Aumayr, K,, Zimmer, M. & Vaziri, A. Brain-wide 3D imaging of neuronal activity in *Caenorhabditis elegans* with sculpted light. *Nat Methods* 10, 1013-1020 (2013).

3. Kato, S., Kaplan, H. S., Schrödel, T. Skora, S. Lindsay, T. H., Yemini, E., Lockery, S. and Zimmer, M. Global brain dynamics embed the motor command sequence of *Caenorhabditis elegans*. *Cell* 163, 656-669 (2015).

4. Nguyen, J. P., Shipley, F. B., Lider, A. N., Plummer, G. S., Liu, M., Setru, S. U., Shaevitz, J. W. & Leifer, A. M. Whole-brain calcium imaging with cellular resolution in freely behaving *Caenorhabditis elegans*. Proc. *Nati. Acad. Sci. USA* 113(8) 1074-1081 (2016).

5. Bruno, A. M., Frost, W. N. & Humphries, M. D. Modular deconstruction reveals the dynamical and physical building blocks of a locomotion motor program. *Neuron* 86(1), 304-318 (2015).

27

1   6. Hill, E. S. Vasireddi, S. K., Wang, J., Bruno, A. M. & Frost, W. M. Memory

2   formation in *Tritonia* via recruitment of variably committed neurons. *Curr. Biol.* 25

3   2879-2888 (2015).

4   7. Hill, E. S., Bruno, A. M. & Frost, W. N. Recent developments in VSD imaging of

5   small neuronal networks. *Learn. Mem.* 86(1). 499-505 (2014).

6   8. Briggman, K. L., Abarbanel, H. D. I. & Kristan, W. B. Optical imaging of neuronal

7   populations during decision-making. *Science* 307, 896-901(2005).

8   9. Briggman, K. L. & Kristan, W. B. Imaging dedicated and multifunctional neural

9   circuits generating distinct behaviors. *J. Neurosci.* 26(42). 10925-10933 (2006).

10   10. Frady, P., Kapoor, A., Horvitz, E. & Kristan, W. B. Scalable semisupervised

11   functional neurocartography reveals canonical neurons in behavioral networks. *Neural*

12   *Comp.* 28(8). 1453-1497 (2016).

13   11. Pipkin, J. E., Bushong, E. A., Ellisman, M. H. & Kristan, W. B. Patterns and

14   distribution of presynaptic and postsynaptic elements within serial electron microscopic

15   reconstructions of neuronal arbors from the medicinal leech *Hirudo verbena*. *J. Comp.*

16   *Neurol.* 524(18). 3677-3695 (2016).

17   12. Kristan, W. B. M., Calabrese, R. L. & Friesen, W.O. Neuronal control of leech

18   behavior. *Prog. Neurobiol.* 76. 279-327 (2005).

28

13. Wagenaar, D. A. An optically stabilized fast-switching light emitting diode as a light source for functional neuroimaging. *PloS ONE*. 7(1). E29822 (2012).

14. Woodford, C. R. Frady, E. R., Smith, R. S., Morey, B., Canzi, G., Palida, S. F., Aranda, R. C., Kristan, W. B., Kubiak, C. P., Miller, E. W. & Tsien, R. Y. Improved PeT molecules for optically sensing voltage in neurons. *J. Am. Chem. Soc*. 137. 1817-1824 (2015).

15. Wagenaar, D. A. & Potter, S. M. Real-time multi-hannel stimulus artifact suppression by local curve fitting. *J. Neurosci. Methods*. 120(2). 113-120 (2002).

16. Lippert, M., Takagaki, K., Xu, W., Huang X. & Wu, JY. Methods for voltage-sensitive dye imaging of rat cortical activity with high signal-to-noise ratio. *J. Neurophisol*. 98(1). 502-512 (2007).

17. Lockery, S. & Kristan, W. B. Distributed processing of sensory information in the leech. II. Identification of Interneurons contributing to the local bending reflex. *J. Neurosci*. 10(6). 1816-1829 (1990).

18. Baljon P. L. & Wagenaar, D. A. Response to conflicting stimuli in a simple stimulus-response pathway. *J. Neurosci*. 35(5) 2398-2406 (2015).

19. Kristan, W. B. Sensory and motor neurons responsible for the local bending response in leeches. *J. Exp. Biol*. 96. 161–180 (1982).

1   20. Gu, X., Muller, K. & Young, S. Synaptic integration at a sensory-motor reflex in the

2   leech. *J. Physiol*. 441. 733-754 (1991).

3   21. Kohsaka, H., Guertin, P. A. & Nose, A. Neural circuits underlying fly larva

4   locomotion. *Curr. Pharm. Des*. 23. 1722-1733 (2017)

5   22. Lewis, J. E. & Kristan, W. B. A neuronal network for computing population vectors

6   in the leech. *Nature* 391. 76–79 (1998).

7   23. Lewis, J. E. & Kristan, W. B. Representation of touch location by a population of

8   leech sensory neurons. *J. Neurophysiol*. 80. 2584–2592 (1998).

9   24. Lewis, J. E. & Kristan, W. B. Quantitative analysis of a directed behavior in the

10   medicinal leech: implications for organizing motor output. *J. Neurosci*. 18. 1571–1582

11   (1998).

12   25. Lewis, J. E. Sensory processing and the network mechanisms for reading neuronal

13   population codes. *J. Comp. Physiol. A*. 185. 373–378 (1999).

14   26. Thomson, E. E. & Kristan, W. B. Encoding and decoding touch location in the leech

15   CNS. *J Neurosci*. 8009-8016 (2006).

16   27. Kretzberg, J., Pirschel, F., Fathiazar, E. & Hilgen, G. Encoding of tactile stimuli by

17   mechanoreceptors and interneurons of the medicinal leech. *Front. Physiol*. 7(506) doi*

18   10.3389/fphys.2016.00506 (2016).

1   28. Wagenaar, D. A., 2017. VScope - A software package for the acquisition and

2   analysis of data from multiple cameras as well as electrophysiology.

3   https://doi.org/10.5281/zenodo.437901. Manuscript submitted.

4   29. Taylor, A. L., Cottrell, G. W., Kleinfield, D. & Kristan, W. B. Imaging reveals

5   synaptic targets of a swim-terminating neuron in the leech CNS. *J. Neurosci.* **23**(36)

6   11402-11410 (2003).

7   30. Cacciatore, T. W., Brodfuehrer, P. D., Gonzalez, J. E., Jiang, T., Adams, S. R.,

8   Tsien, R. Y., Kristan, W. B. & Kleinfeld, D. Identification of neural circuits by imaging

9   coherent electrical activity with FRET-based dyes. *Neuron* **23**. 449-459 (1999).
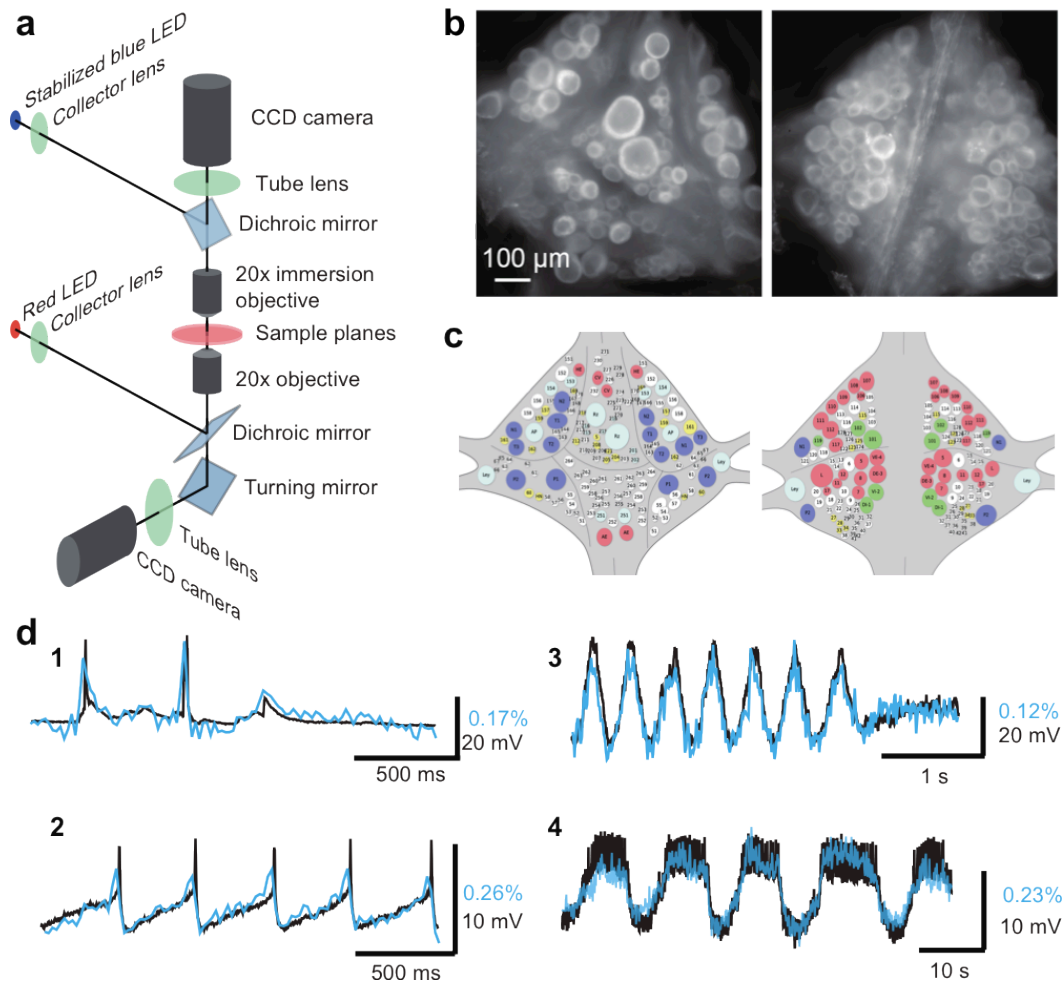
10

11

12

1 **Acknowledgments**

9

10 **Competing Interests**

11 The authors declare no competing interests.

12

1 **Figures**

2 Figure 1

4 **Figure 1 |** Double-sided voltage sensitive dye imaging. **(a)** Schematic of the

5 double-sided microscope. **(b)** Images of the ventral (*left*) and dorsal (*right*) aspects of a

6 leech ganglion simultaneously acquired using this microscope. **(c)** Canonical maps of

7 the ventral (*left*) and dorsal (*right*) aspects of the ganglion. **(d)** Single-sweep recordings

8 of neuronal activity. Optical signals from VSD imaging (*blue*) are overlaid with

9 simultaneous intracellular recordings (*black*). **1.** Action potentials and subthreshold

1   potentials in a Retzius cell; **2.** Spontaneous regular firing in an AP cell; **3.** Swimming

2   pattern in a DE-3 motor neuron; **4.** Crawling pattern in an AE cell.

3
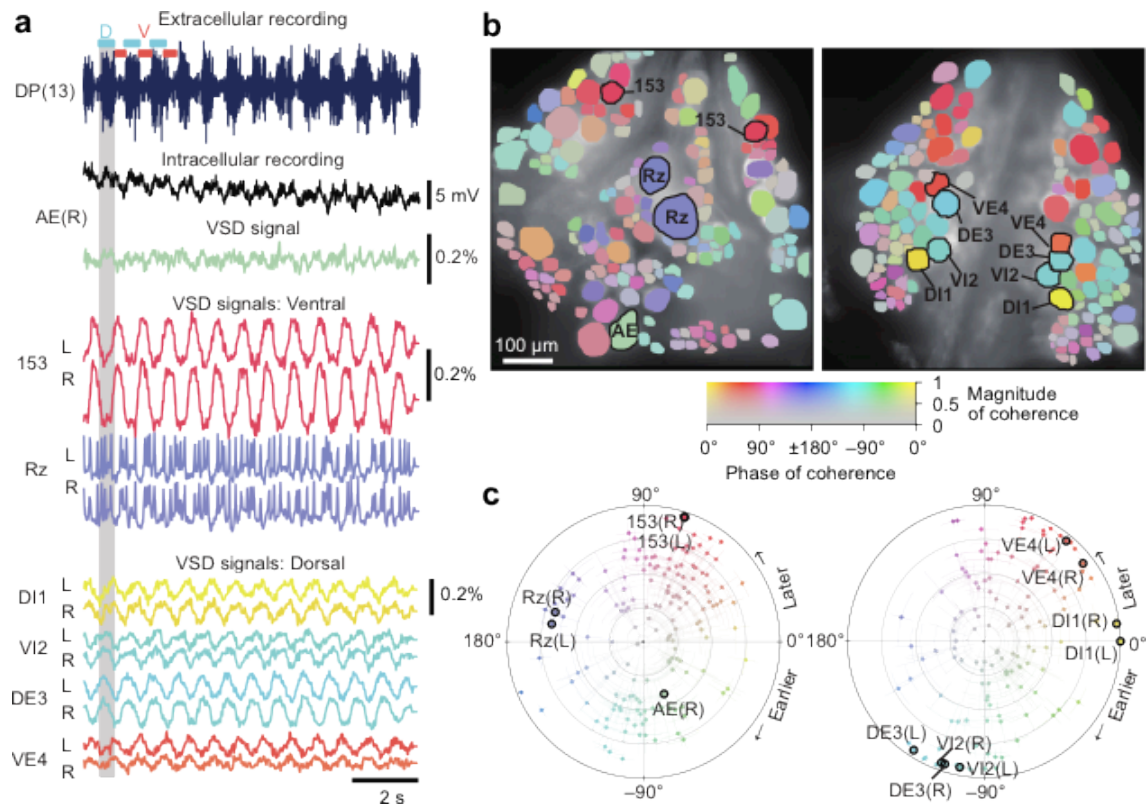
1   Figure 2

3   **Figure 2 |** Neuronal activity during fictive swimming. **(a)** Selected electrophysiological

4   and VSD traces during fictive swimming. Extracellular recording from a nerve root in a

5   posterior segment (DP(13)) showed rhythmic dorsal motor neuron bursts characteristic

6   of swimming (*top*). Intracellular recording and simultaneous optical signal from an AE

7   neuron show matching membrane potential oscillations. VSD signals from the ventral

8   surface: bilateral cells 153 (a sensory neuron) and the Retzius cell (a neuromodulatory

9   neuron). VSD signals from the dorsal surface: dorsal and ventral inhibitory and

10   excitatory motor neurons DI-1, VI-2, DE-3, and VE-4. **(b)** Coherence of the optically

11   recorded signals of all cells on the ventral (*left*) and dorsal (*right*) surfaces of the

12   ganglion with the swim rhythm. Cells used in **(a)** are marked. **(c)** Magnitude (radial axis

13   from 0 to 1) and phase (angular coordinate) of the coherence of each neuron's activity

35

1   with the swim rhythm; same data as in **(b)**. Error bars indicate confidence intervals

2   based on a multi-taper estimate.

3

1   Figure 3
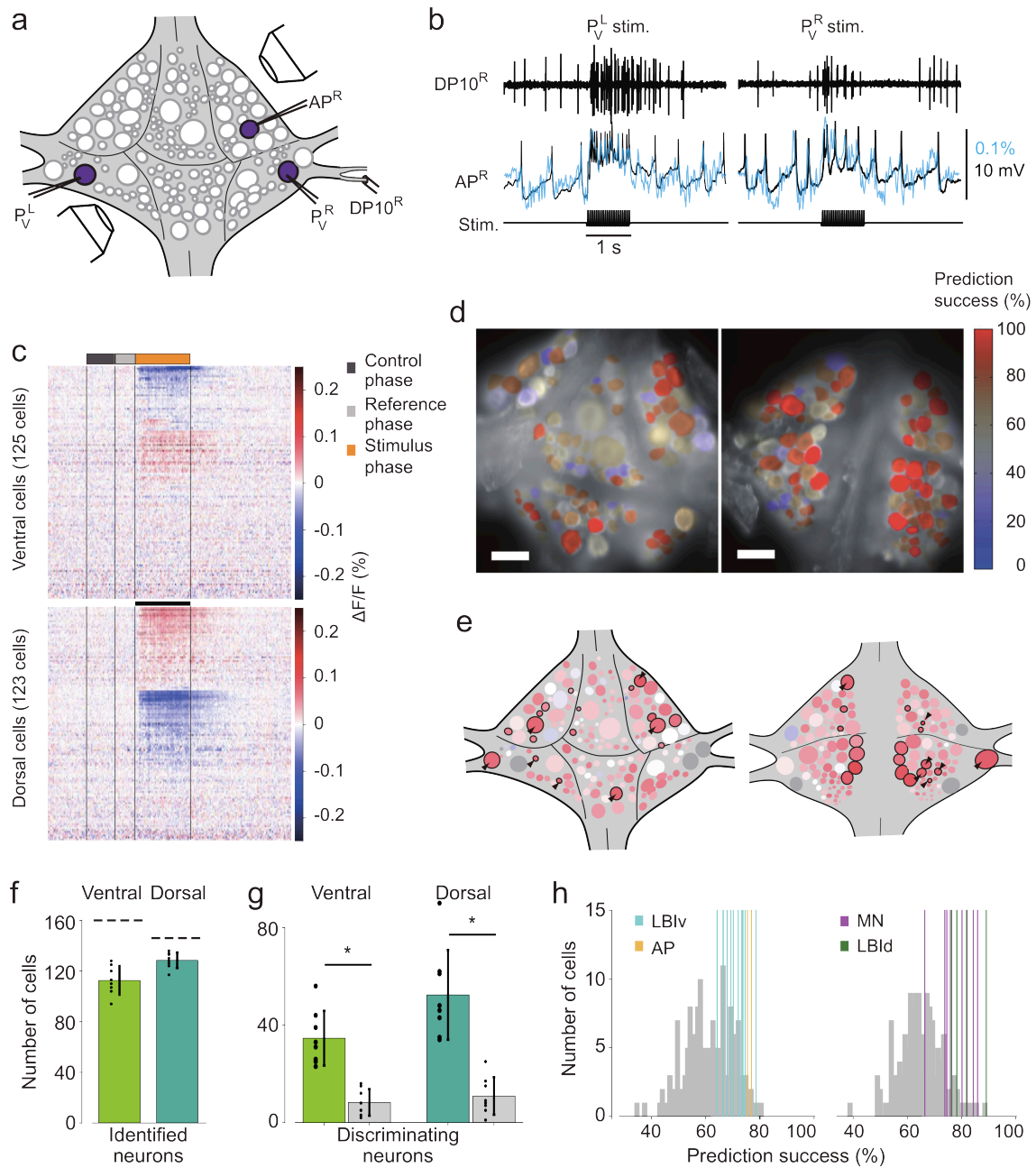
2

3   **Figure 3 |** Differential activation during left and right local bend responses. **(a)**

4   Schematic of the setup. Microelectrodes were inserted into left and right P_V cells for

5   stimulation and into the right AP cell for recording. A suction electrode around the right

6   DP nerve confirmed the execution of a (fictive) local bend. **(b)** Simultaneously recorded

1   motor activity from the DP nerve (*top*), membrane potential from the AP neuron

2   (*middle*, *black*) and its corresponding VSD trace (*blue*) in response to stimuli to P_V^L

3   (*left*) and P_V^R (*right*). Stimulus duration was 1 second (*bottom*). **(c)** Time series of

4   averaged difference between P_V^L ($n = 10$) and P_V^R ($n = 10$) trials in the activity of all 248

5   recorded cells. Positive (*red*) indicates more depolarization (or less hyperpolarization)

6   in response to P_V^R stimulation. Scale bar: 1 second. **(d)** Stimulus discriminability score

7   overlaid on images of the ventral (*left*) and dorsal (*right*) aspects of the ganglion. Scale

8   bars: 100 μm. **(e)** Averaged discriminability results across 8 animals. Color scale as in

9   **(d)**. Motor neurons (MNs) and LBIs are marked (*black circles*) as are other cells that

10   strongly discriminate between stimuli ($\geq$ 75% prediction success; *circles and arrow*

11   *heads*). **(f)** Number of cells that could be mapped to identified neurons; mean and SD of

12   8 preparations and individual results (*dots*). Dashed lines indicate total number of cells

13   in the canonical maps. **(g)** Number of cells that strongly discriminate between stimuli ($\geq$

14   75% prediction success) compared to control (*grey bars*). (*: $p < 10^{-4}$; Paired sample

15   T-test) **(h)** Discriminability scores for all neurons on the ventral (*left*) and dorsal (*right*)

16   surfaces. Colored lines mark the scores of LBIs, AP cells and MNs.
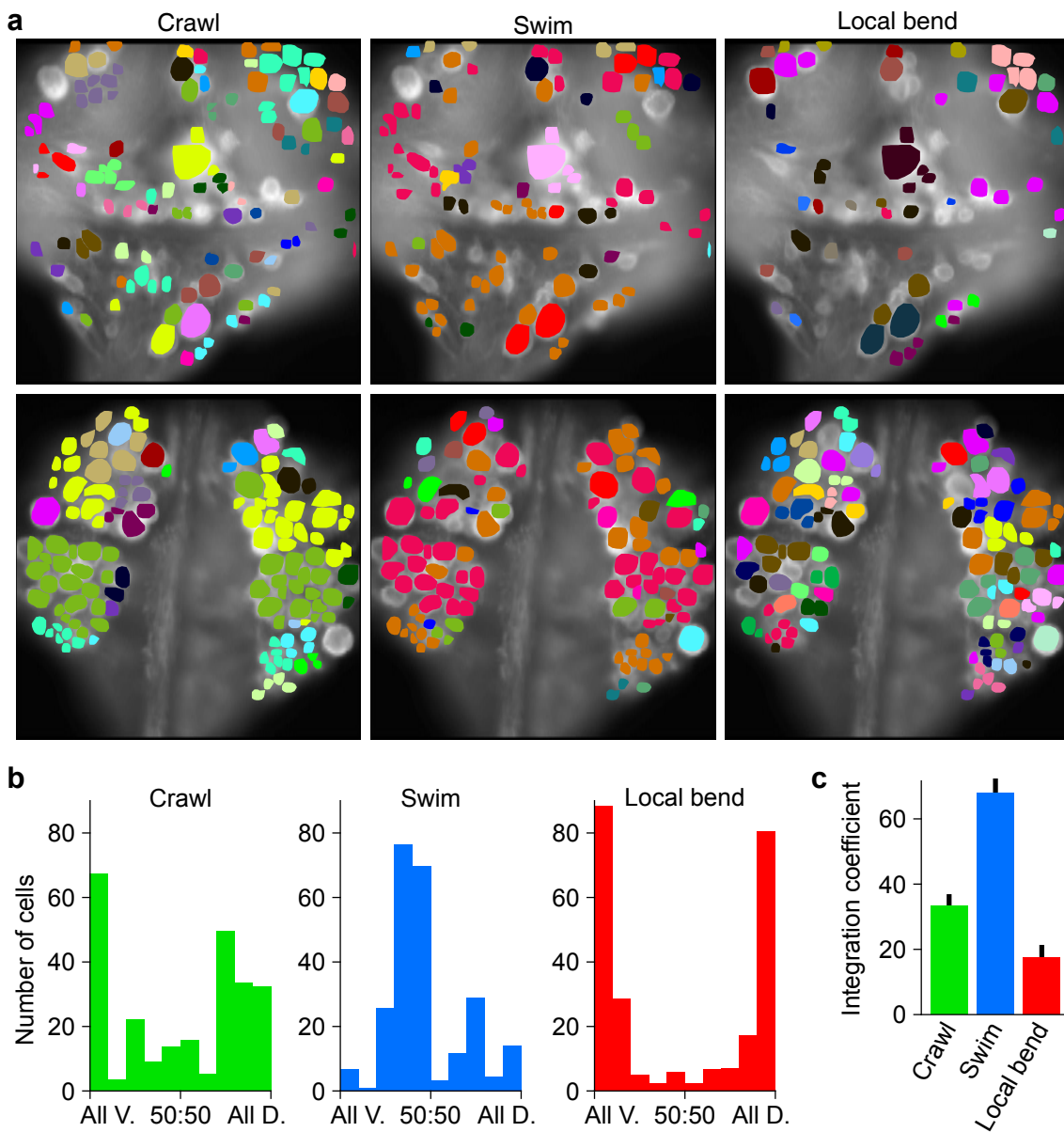
1   Figure 4
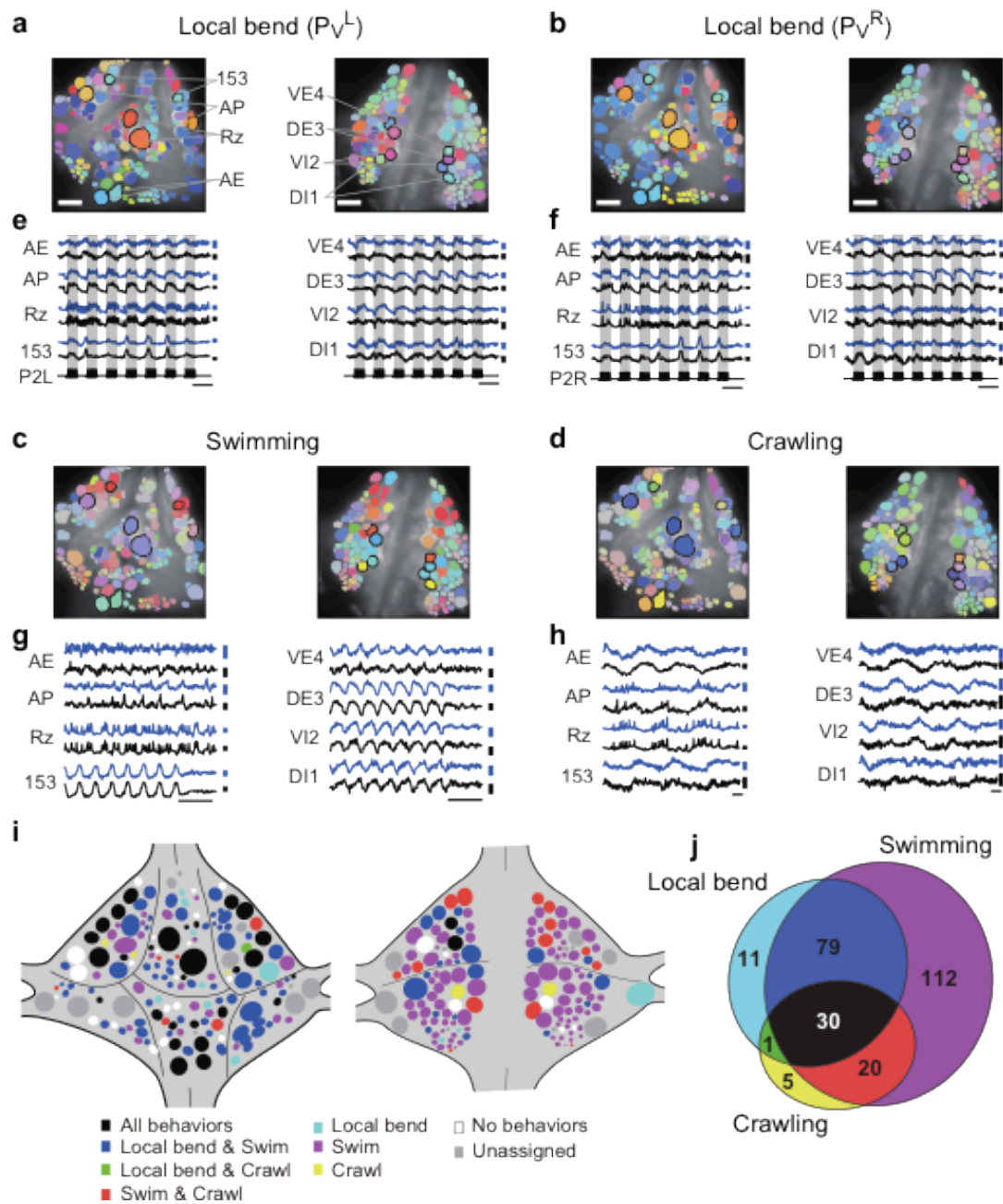
2

3   **Figure 4 |** Neuronal activity during multiple behaviors. **(a–d)** Coherence of optically

4   recorded signals of all cells on the ventral (*left*) and dorsal (*right*) surfaces of a ganglion

5   with **(a)** P_V^L-induced local bending, **(b)** P_V^R-induced local bending, **(c)** fictive swimming,

6   and **(d)** fictive crawling. Color map as in Fig. 2b. **(e-h)** VSD signals of cells indicated in

1   **(a–d)** during those behaviors. **(i)** Summary maps of the involvement of identified

2   neurons on the ventral (*left*) and dorsal (*right*) surface of the ganglion. Colors indicate

3   which behavior each neuron was involved in. **(j)** Venn diagram showing the total

4   number of identified neurons that oscillated with each individual behaviors or

5   combinations of behaviors. Colors as in **(i)**.

6

1   Figure 5

2

3   **Figure 5** | Clustering cells based on their activity in different behaviors. **(a)** Cluster

4   assignments of all cells recorded in one animal based on the correlation matrix of their

5   activity during fictive crawling (*left*), swimming (*center*), and local bending (*right*). **(b)**

6   Degree to which cells within a cluster were fully contained on the ventral side ("All

7   V."), fully on the dorsal side ("All D."), or equally distributed ("50:50"). To prevent

1   overrepresentation of small clusters, each cell is an entry in the histogram, not each

2   cluster. Clusters with fewer than 3 members were excluded. Data from $N = 6$ leeches.

3   **(c)** Quantification of the degree to which members of clusters were distributed across

4   surfaces in the three behaviors tested (mean ± SEM, $N = 6$). All differences were

5   significant (ANOVA, $F(2,15) = 63.4$, $p < 10^{-7}$, followed by Tukey).